Asociación Argentina
de Mecánica Computacional

Mecánica Computacional Vol XXVIII, págs. 1641-1660 (artículo completo)
Cristian García Bauza, Pablo Lotito, Lisandro Parente, Marcelo Vénere (Eds.)
Tandil, Argentina, 3-6 Noviembre 2009

CFD STUDY OF FLOW DISTRIBUTION AND WETTING EFFICIENCY OF THE PERFORATED TRAY DISTRIBUTOR OF A TRICKLE BED REACTOR

D. Ramajo[a], M. Raviculé[b], M. Monsalvo[b], S. Marquez Damian[a], M. Storti[a] and N. Nigro[a]

[a]*International Center for Computational Methods in Engineering (CIMEC)*
INTEC-UNL-CONICET, Güemes 3450, Santa Fe, Argentina, dramajo@santafe-conicet.gov.ar

[b]*Centro de Tecnología Argentina (CTA), YPF, Baradero s/nro. 1925, Ensenada, Argentina,*
mravicules@ypf.com

Keywords: tray efficiency, trickle bed reactor, petrochemical, CFD.

Abstract. Trickle bed reactors are massively employed in petrochemical and chemical plants. Reactors consist of one or more beds filled up with catalyst particles. The efficient utilization of the catalyst is dependent on the good distribution of the liquid of the charge across the catalyst beds. On the contrary some parts of the beds will get less liquid reactants while others will get more than the average. In zones where there is maldistribution of reactants the reaction will extent to undesired reactions, leading to deactivation of the catalyst and towards low conversions. Bad tray efficiency due to non-uniform liquid distribution will result in low reactor efficiency and shorten the catalyst's cycle time. The analyzed one is a trickle bed reactor that processes butene (liquid) and hydrogen (gas). The charge is introduced through the upper side and liquid accumulates on the tray to a certain level swamping the perforated plate tray. The liquid phase flows down through 68 small holes while the gas phase descends through 7 chimneys. There is another ceramic-ball bed above the catalyst bed with the aim to get a better distribution of the charge.
In this work a computational fluid dynamics study (CFD) was carried out with the aim to know the wetting efficiency of the tray distributor under different operating conditions. The Eulerian two-fluid model was employed. Because of tray holes are very small with respect to the overall tray, drains and sources were employed to represent them. In this sense, numerical and experimental models were employed to know the response mass flow rate versus liquid height for the holes.
Little differences on the mass flow rate across the holes were found because of the scarce liquid sloshing above the tray. Due to the small gas fraction of the charge, the liquid flows only by gravity so it is not sprayed after leaving holes and the extent of the wetted zone below each drip point (hole) is small. A suitable correlation to estimate the expansion of the wetted zone caused by the ceramic-ball bed was employed, showing that all the top catalyst bed side is wetted but significant differences on liquid concentration are found. Nevertheless, the wetting

Copyright © 2009 Asociación Argentina de Mecánica Computacional http://www.amcaonline.org.ar

distribution from CFD seems not be as bad as to explain the low overall efficiency of the reactor. So, an additional possible cause of low efficiency can be found on fouling and obstruction of some holes.
Although more efficient distribution trays are currently employed in trickled bed reactors (eg. bubble cap trays) they need higher gas flow rates to work. Only chimney trays are capable to diminish fouling problems but on the other hand, due to its larger size, the number of drip points will be reduced. Two simple geometric modifications are proposed to enhance tray performance, firstly to reduce the amount of gas chimneys from 7 to only one, adding additional drip points, secondly to replace the holes for short risers in order to reduce the vulnerability to plugging.

1 INTRODUCTION

Fixed-bed reactors operating under trickle-flow conditions (TBRs) are massively employed in hydrotreating processes petroleum refineries, petrochemical plants and in many gas-liquid-solid reactions of the chemical industry. The analyzed TBR is a multiphase (gas-liquid-solid) catalyst reactor in which gas and liquid phases flow cocurrently downward through a fixed bed of solid catalyst particles.
Since the introduction of fixed-bed hydroprocessing technology in the early 1950's significant improvements on catalyst efficiency have been made. But in the mid 1990's it become apparent that the design of hydroprocessing reactors had not advanced at the same pace as the development of hydroprocessing catalysts. As a result, licensors began to develop high performance reactor internals. Of course, technologies are licensed and scarce information about their behavior is available (Ranade, 2002).
There are three crucial issues affecting reactor efficiency; effective catalyst utilization, optimum gas/liquid distribution, and low radial temperature differences. It is known that liquid flow maldistribution in TBR is responsible for creating damaging hot spots, which are observed by thermocouple measurements. A good design of the liquid distributor is one of the important factors to prevent liquid maldistribution in industrial scale reactors. However, though uniform liquid distribution is achieved at the distributor, significant bypassing (channeling) and/or segregation could occur due to the improper way in which catalyst and fines are packed (Wu and Dudukovic, 1995). For example, a 2.5% flow bypass in a single-bed reactor with a 2 wt% sulfur content feedstock would lead to a product containing at least 500 ppm of sulfur (Harter et al., 2001).
The literature on liquid distribution is scanty as compared to that on other hydrodynamic parameters. The most of them focused on study the flow distribution within the catalyst bed (Lopes and Quinta-Ferreira, 2008; Gunjal et al., 2005; Kundu et al., 2001), and a few dealing with the distributors and trays efficiency (Maiti and Nigam, 2007; Harter et al., 2001). Finally, some of them study the effect of the distributor over the liquid behavior inside the catalyst bed (Atta et al., 2007).
Regarding perforated-plate trays, they are vulnerable to plugging by solid particles entering to the reactor, coke or corrosion products. Moreover, small tray levelness caused during installation can also lie to loss of efficiency (Alvarez et al., 2007; Maiti et al., 2007).
Computational fluid dynamics (CFD) is beginning to be employed as a useful tool for helping developers to design more efficient liquid distributors (Harter et al., 2001). In this work the entry device and perforated-plate tray of a fixed-bed TBR was studied by CFD. Investigation

Copyright © 2009 Asociación Argentina de Mecánica Computacional http://www.amcaonline.org.ar

was focused to understand the two-phase fluid flow behavior and the tray wetting efficiency. Perforated-plate tray holes were modeled using sink and source points, and the effect of the ceramic-ball bed above the catalyst bed was estimated by an empirical equation. These techniques allowed the simulation of the overall entry device with a relatively low computational cost.

2 METHODOLOGY

2.1 Reactor characteristics

The TBR operate in plug flow regime. The inlet charge is a mixture of mainly butene (liquid) and small fractions of hydrogen (both gas and liquid depending on the operating conditions) that is injected 4 meters upstreams the TBR. Charge drops onto the tray distributor from a central inlet distributor flooding the tray. Figure 1 shows the geometry of the entry device of the TBR. The inlet distributor is a cylinder with 5 equidistant vertical slots and 15 holes on the bottom side. The perforated-plate of the tray consists of 7 chimneys for gas flow and 68 holes for liquid flow. Liquid swamps the tray to a certain level and flow through holes by gravity. Below the tray and above the catalyst bed there is a ceramic-ball bed (ball diameter = ¾ inch, bed height = 150 mm) that has the function to enhance liquid distribution. Figure 2 shows a view of the tray from the top. As noted, holes are placed over a rhomboidal lattice while chimneys are radially distributed. The inlet duct is also indicated with dashed lines.

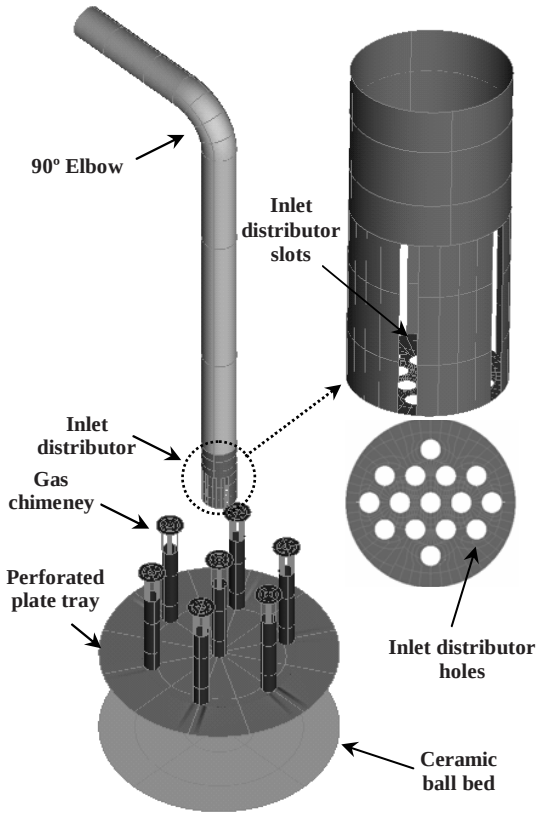

Figure 1: Geometry of the entry device and tray distributor.

Copyright © 2009 Asociación Argentina de Mecánica Computacional http://www.amcaonline.org.ar

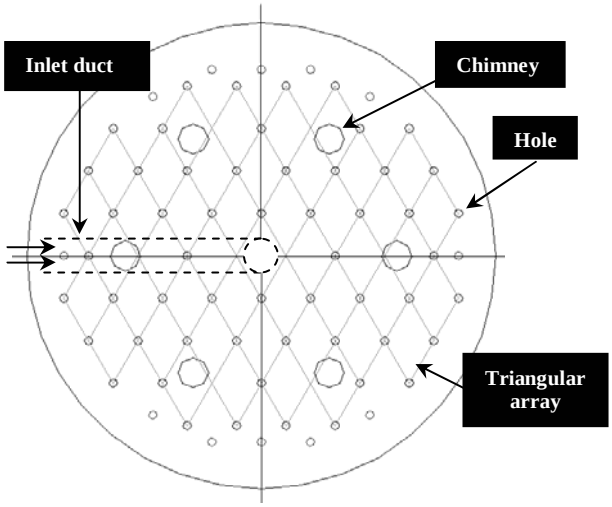

Figure 2: Geometry of the tray showing the 68 holes and the 7 chimneys.

Operating conditions and fluid properties of the TBR change in function of the catalyst ageing and its progressive deactivation. Table 1 shows the data employed for simulation, corresponding to the beginning of catalyst life cycle. For aged catalyst temperature and pressure are increased in order to hold conversion efficiency, that leading to negligible gas (hydrogen) at inlet.

Temperature	44.5 ºC
Pressure	11.3 kg/cm^2
Liquid	
Mass flow rate	12447 kg/h
Density	565.6 kg/m^3
Dynamic viscosity	0.135 centipoise
Surface tension	9.78 dyn/cm
Gas	
Mass flow rate	8.3 kg/h
Density	10.2 kg/m^3
Dynamic viscosity	0.012 centipoise

Table 1: Operating conditions and fluid properties.

2.2 Computational model

The computational domain was meshed with 1.845.274 tetrahedric elements and 345.219 mesh nodes. Only the entry device of the overall TBR was modelled. Figure 3 shows the corresponding surface mesh. As noted, mesh was locally refined around the inlet distributor and gas chimneys.

Copyright © 2009 Asociación Argentina de Mecánica Computacional http://www.amcaonline.org.ar

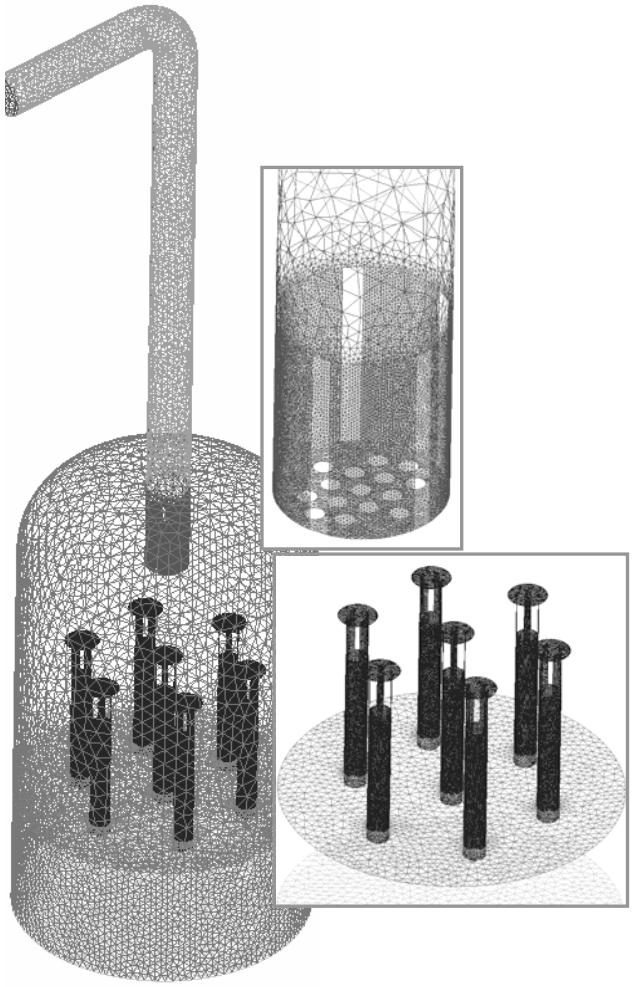

Figure 3: Surface mesh of the computational model.

The unsteady multi-fluid formulation using the two-fluid model was employed for simulation. As it is well known from theory, in this formulation single phase Navier-Stokes equations are modified according to some sort of regularization or average to model the small scales, introducing the volume fraction of each phase along with appropriate terms considering the mass, momentum and energy transferred through the interface among the phases. Since no reactions take place at the entry device of the TBR, the problem was modelled as isothermal. Continuity equation for α phase is:

$$\frac{\partial(\delta_\alpha \rho_\alpha)}{\partial t} + \nabla \bullet \left(\delta_\alpha \rho_\alpha \vec{U}_\alpha\right) = S_\alpha + \sum_{\beta \neq \alpha} \Gamma_{S,\alpha\beta} \quad \text{and} \quad \sum_\alpha \delta_\alpha = 1 \tag{1}$$

where δ_α is the volume fraction, ρ_α the density, S_α the mass sources or sinks, $\vec{U}_\alpha$ the velocity and $\Gamma_{S,\alpha\beta}$ the interfacial mass transfer. Note from Eq. (1) that the summatory of the volume fraction of all phases must be 1, it being a constrain condition. Regarding the momentum equation, it can be written as:

Copyright © 2009 Asociación Argentina de Mecánica Computacional http://www.amcaonline.org.ar

$$\frac{\partial}{\partial t}\left(\delta_\alpha \rho_\alpha \vec{U}_\alpha\right) + \nabla \bullet \left(\delta_\alpha \left(\rho_\alpha \vec{U}_\alpha \otimes \vec{U}_\alpha\right)\right) = -\delta_\alpha \nabla P + \nabla \bullet \tau_\alpha + \delta_\alpha \varphi_\alpha + S_{M\alpha} + \sum_{\beta \neq \alpha} M_{\alpha\beta} + \sum_{\beta \neq \alpha} \Gamma_{M,\alpha\beta} \qquad (2)$$

where P is the static pressure (shared for all phases), τ_α is the shear stress tensor, φ_α is the external volumetric momentum source (potential force fields, i.e. gravity), $S_{M\alpha}$ are momentum sources and $M_{\alpha\beta}$ is the interfacial force caused by the presence of others phases, commonly divided between drag and non-drag forces. Finally $\Gamma_{M\alpha\beta}$ are the net momentum quantities transferred at the interface between α and β phases by phase change. In this work both $\Gamma_{S,\alpha\beta}$ in Eq. (1) and $\Gamma_{M\alpha\beta}$ were not taking into account while S_α and $S_{M\alpha}$ were employed to represent tray holes by sink and source of mass and momentum.

A k-ε model was employed to model turbulence and a standard logarithm wall law was applied near walls.

Regarding time integration a first order backward Euler scheme was applied. Several time steps from 0.001 sec. to 0.01 sec. were considered, being 0.005 sec. the maximum time step that guarantied a RMS convergence criterion for equation residual less than $1x10^{-6}$. The problem was solved using distributed computing facilities over several processors in a Beowulf cluster (Storti et al., 2002; Sonzogni et al., 2002).

The mass flow rate for both phases and the turbulence intensity (5%) was set at inlet. The surface of the ceramic-ball bed was represented by an opening condition with a static pressure equal to the reactor operation pressure (11.3 kg/cm^2), that allows both phases can leave the domain but only the gas phase can enter to it. Finally, walls were set as no slip with null roughness. Simulations were initialized with a liquid level over the tray that was estimated based on a correlation for the discharge mass flow rate through a hole in a flat plate (Eq. (3)).

2.3 Reduced tray models

Tray-hole diameter is only 10 mm while the tray diameter is around 570 mm. That means holes are difficult to be represented on the computational domain due to the size scales involved. Besides, the amount of holes is large (68) and the tray thickness is only 8 mm. So, in order to gain some insight into the tray hole modelling three reduced models, considering only one gas chimney and 12 tray holes, were employed to evaluate different options to represent the holes. Firstly, considering a non-thickness perforated-plate tray. Secondly, a perforated-plate tray with the real thickness (8 mm). Thirdly, a blind-plate tray representing the holes as local mass and momentum sinks above the tray and sources below it. Fluid properties were those of the real TBR, while the mass flow rate for liquid and gas phases was proportional to the amount of holes and chimneys respectively. Figure 4 shows the models mentioned above.

Copyright © 2009 Asociación Argentina de Mecánica Computacional http://www.amcaonline.org.ar

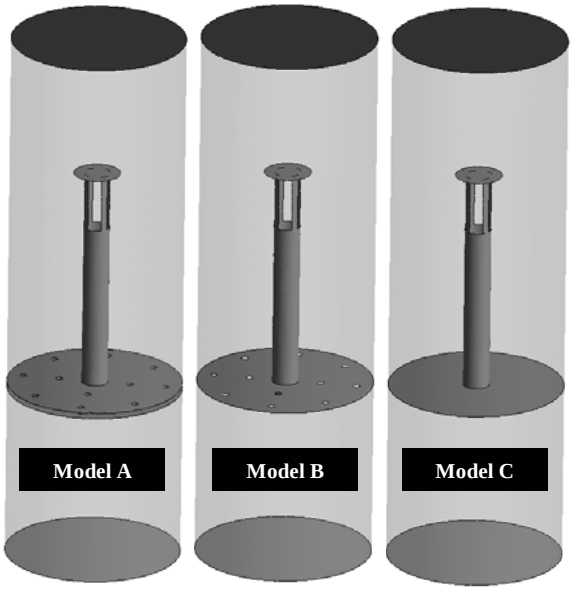

Figure 4: Reduced tray models.

Table 2 displays the mesh sizes of the three reduced models. Note that the mesh size of model C is around a half of model A, while model B is in the middle. Moreover, a better mesh quality was observed for model C.

	Model A	**Model B**	**Model C**
Elements	1.104.669	869.370	546.724
Nodes	198.229	153.209	98.925

Table 2: Mesh size for the three reduced models.

Boundary conditions for reduced models were the same that the explained above for the overall entry-device model except for the lateral cylindrical boundary that was set as free slip. For model C, mass sinks were located 5 mm above the tray and mass and momentum sources were located 5 mm below it. The following correlation for the discharge through a hole was considered:

$$\dot{m} = C.A.\sqrt{2\vec{g}\rho^2\left(H_0 - \frac{(P-P_0)}{\vec{g}\rho}\right)} \tag{3}$$

where A is the cross sectional area of the hole, ρ is the liquid density, H_0 and P_0 are reference height and pressure, P is the pressure proved at each sink position $\vec{g}$ is the gravity and C is a shape coefficient that mainly depend on the shape of the hole edges (sharp or rounded) and the ratio between the diameter and the thickness of the hole. Note that in Eq. (3) only the fluid density is taken into account. Viscosity, surface tension or any other rheological fluid parameter is neglected. However, it must be noted that flow through small holes is strongly turbulent, so the wall frictional coefficient and C coefficient become nearly the same for almost all fluids.

Copyright © 2009 Asociación Argentina de Mecánica Computacional http://www.amcaonline.org.ar

Based on reported data (Dally et al., 1993; Perry et al., 1984) C coefficient ranges from 0.6 to 0.8, but it was not found a suitable coefficient for the studied hole geometry, so *CFD* and experimental tests were carried out to estimate it.

3 RESULTS

3.1 Shape coefficient C for modeling the holes

Numerical simulation

Figure 5 shows the computational axysimmetric model of a hole. Due to symmetry conditions and to reduce computational cost, only 15º of the 360º overall hole was modeled. Simulation was aimed to reproduce the discharge of liquid through a hole on the bottom of a recipient with an initial liquid level of 0.3 m.

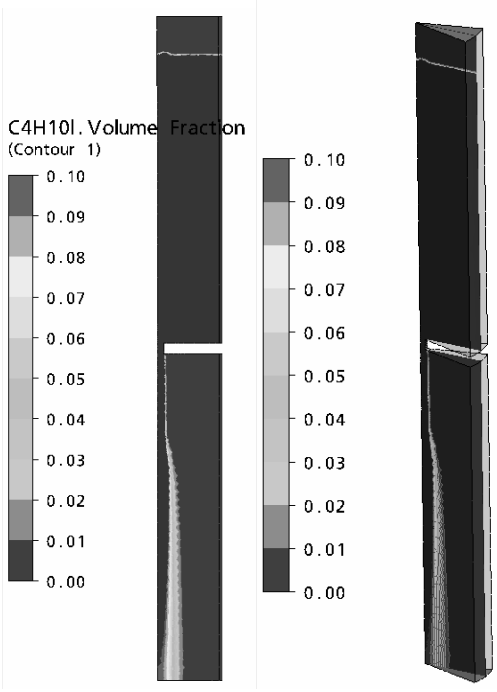

Figure 5: Axisymmetric computational model of a hole.

Figure 6 shows the evolution of the mass flow rate $\dot{m}$ and the liquid level height h_f along the simulation. Note that $\dot{m}$ linearly reduces with time while h_f reduces following a second order-polynomial-time relation.

Copyright © 2009 Asociación Argentina de Mecánica Computacional http://www.amcaonline.org.ar

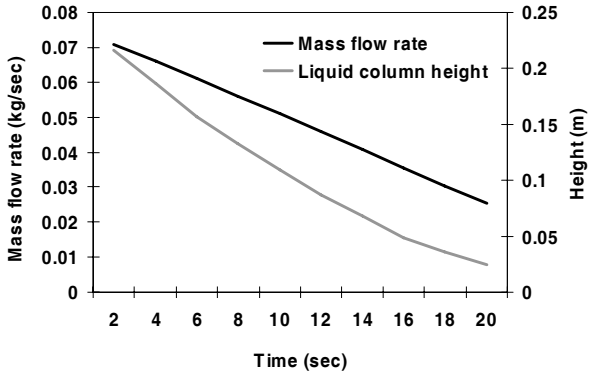

Figure 6: Mass flow rate $\dot{m}$ and liquid level height h_f during discharge.

To probe the pressure in a point above the hole is easier than to estimate the liquid level height h_f. So, it is more convenient to express h_f as a function of a reference pressure P_0 at a reference height h_0 and the pressure at a monitor point (see Eq. (3)). Then, Eq. (3) allows to find the shape coefficient C that better fit test results, it being 0.77. Figure 7 shows the mass flow rate in function of the manometric hydrostatic pressure at the monitor point (5 mm above the hole) along with the results corresponding to Eq. (3) for C = 0.77. As noted, CFD and Eq. (3) results are in fair agreement.

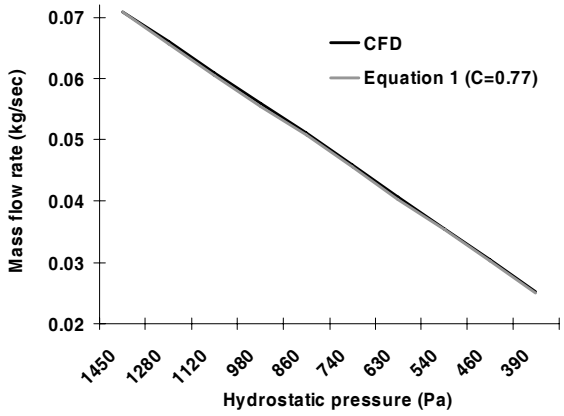

Figure 7: Mass flow rate as a function of the manometric hydrostatic pressure at 5 mm above the hole.

Experimental test

In contrast with the numerical simulation, the experiment test was carried on with water, measuring the mass flow rate for several constant liquid level heights. It is rather different from the numerical simulation in witch liquid properties corresponded to butene and regime was transient because the liquid level height was not keep constant.

The coefficient C by the experimental test was 0.72, this being 6.5% less than the numerical one. Differences between the numerical and experimental test methodology could justify discrepancies. During the experimental test it was observed that the flow rate is strongly influenced by the turbulence around the hole produced by the flow realimentation from the top

Copyright © 2009 Asociación Argentina de Mecánica Computacional http://www.amcaonline.org.ar

of the device (realimentation inlet is at 350 mm above the hole). At high liquid level heights the realimentation produces negligible disturbance and agitation of the liquid near the hole, but at liquid level heights around or less than 100 mm the flow rate is notoriously increased, that leads coefficient C to overcome the 0.8 value. Of course, it was not observed for the numerical simulation since realimentation was no considered.

3.2 Reduced tray models

This section shows the results corresponding to the reduced tray models showed in Figure 4. Figure 8 displays the liquid volume fraction at a cross sectional plane for the three models once the global mass balance (between the inlet and the outlet boundaries) for both phases was reached. It is easy to note the significant discrepancies between the results corresponding to model A (thickness perforated-plate) and model B (non-thickness perforated-plate). All simulations started from the same initial liquid level height (120 mm above the plate) but for model B the steady state liquid level became strongly lower than for the other models. Although for the authors it is not clear the cause of this behavior, it is not physically correct due to the fact that the coefficient C for a non-thickness plate must be lower (around 0.6) than for a thickness one. So, wrong results are probably caused by numerical problems.

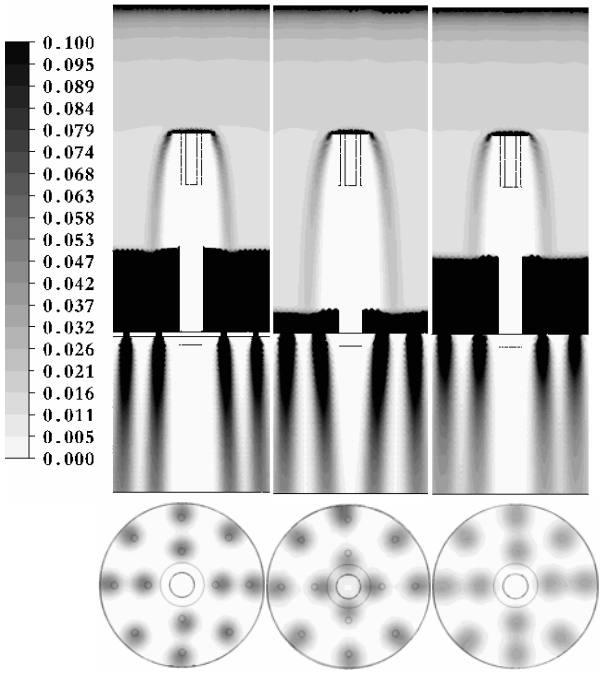

Figure 8: Liquid volume fraction. Left: model A (thickness perforated-plate). Center: model B (non-thickness perforated-plate). Right: model C (blind plate with sink and source points).

Results were fairly similar for models A and C. Figure 9 shows the liquid vertical velocity while Figure 10 shows the corresponding to the gas phase. Liquid velocity is fairly similar above the plate for models A and C, but below the plate the model C results seems to be a bit more dissipative.

Copyright © 2009 Asociación Argentina de Mecánica Computacional http://www.amcaonline.org.ar

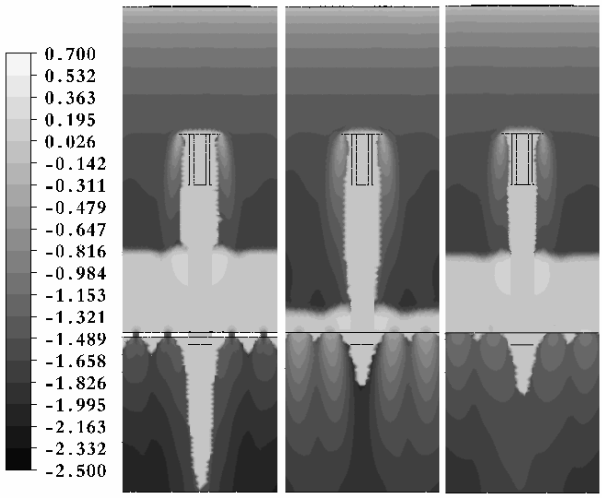

Figure 9: Vertical velocity for liquid phase. Left: model A (thickness perforated-plate). Center: model B (non-thickness perforated-plate). Right: model C (blind plate with sink and source points).

Since the gas mass flow rate is very low the gas motion is mainly caused by gas-liquid drag efforts. As shown Figure 10, the gas goes down along with the liquid below the holes and a significant gas recirculation is found below the chimney.

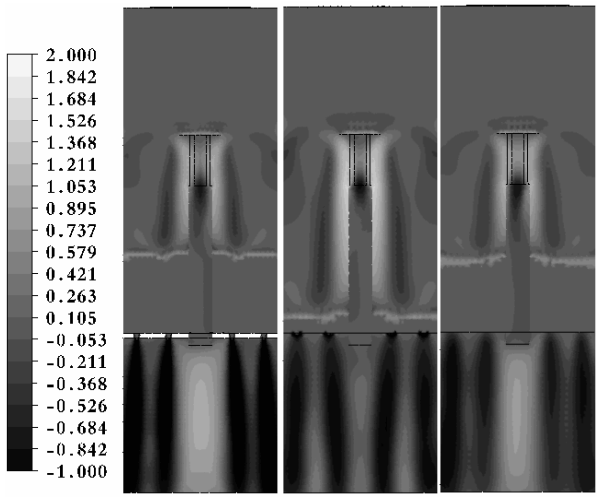

Figure 10: Vertical velocity for gas phase. Left: model A (thickness perforated-plate). Center: model B (non-thickness perforated-plate). Right: model C (sink and source points).

From Figures 8, 9 and 10 it can be concluded that the use of sinks and sources is a suitable option to model holes that are notably smaller than the overall domain.
Regarding the convergence of the global mass balance, gas phase convergence was extremely slow. That may be explained by the fact that the liquid mass flow rate is more than 1500 times higher than the gas one. As it is well known the two-fluid model is not well posed for solving problems involving large differences in the density or the volume fraction or high slip velocities between phases (Zanotti et al., 2007). Besides, when the mass flow rate of one fluid is quite smaller than the others, it is necessary to use double precision solvers and run a large

Copyright © 2009 Asociación Argentina de Mecánica Computacional http://www.amcaonline.org.ar

time period to reduce the relative error in the global mass balance. For model B more than 1.800 time steps were required to reach a global mass balance with a relative error less than 10% while for models A and C more than 10.000 time steps had to be solved to reach an error less than 5%. Gas convergence was slower than the liquid one. After the firsts 5000 time steps the global mass balance error was around 25% but it was necessary to run 5000 time steps more to reduce error to less than 5%.

Table 3 consigns the global mass balance of model C for both phases at three simulation times. As noted, after 43.75 sec. (8750 time steps) the global liquid mass balance error was less than 0.5%. However, an additional period of 8 sec. (1600 time steps that required around 38 hours of computing time using 10 processors) was required to reduce the error to 0.14%. Clearly it is an excessive computational effort. On the other hand, the error corresponding to the gas phase still results significant at 43.75 sec. but is notoriously reduced at 51.75 sec. But, it has negligible effects over the liquid phase, as can be noted from Figure 11 where the volume fraction of liquid is drawn for the three simulation instants consigned in the table. The same conclusion is reached by drawing the gas vertical velocity (see Figure 12).

Time (sec)		Mass flow rate (kg/sec)		Error %
		Inlet	Outlet	
20.0	Liquid	6.1014×10^{-1}	5.8233×10^{-1}	4.6
	Gas	4.0353×10^{-4}	1.0122×10^{-3}	151
43.75	Liquid	6.1014×10^{-1}	6.0745×10^{-1}	0.44
	Gas	4.0353×10^{-4}	4.6373×10^{-4}	14.9
51.75	Liquid	6.1014×10^{-1}	6.0929×10^{-1}	0.14
	Gas	4.0353×10^{-4}	4.2211×10^{-4}	4.61

Table 3: Mass flow rate at inlet and outlet and global mass balance error at three simulation times.

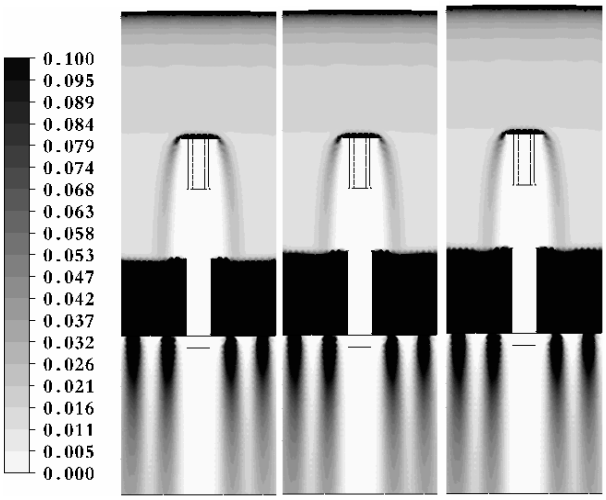

Figure 11: Model C. Liquid volume fraction at three simulation times. Left: 28.25 sec. Center: 36.75 sec. Right: 51.75 sec.

Copyright © 2009 Asociación Argentina de Mecánica Computacional http://www.amcaonline.org.ar

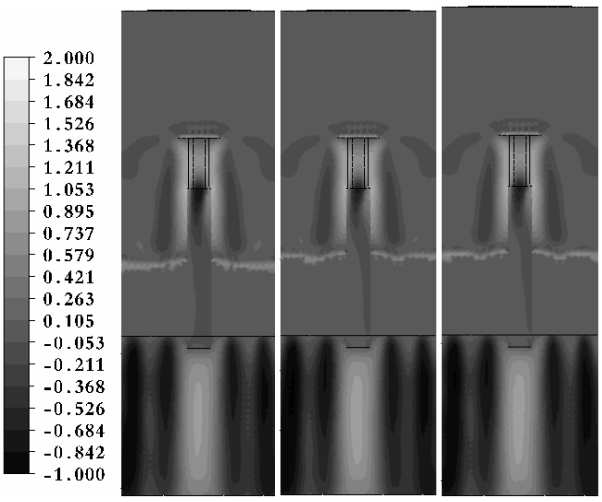

Figure 12: Model C. Gas vertical velocity at three simulation times.
Left: 20 sec. Center: 43.75 sec. Right: 51.75 sec.

Summarising, reducing the error of the global mass balance of phases with very low mass flow rates has a higher computational cost due to model mathematical problems and from the point of view of the results it has irrelevant effects for industrial problems.

3.3 Industrial TBR

The average liquid level height h_{av} for steady state conditions was obtained using the following equation:

$$h_{av} = \frac{1}{2\vec{g}\rho^2}\left(\frac{\dot{m}_{nom}}{N_{ho}.C.A}\right)^2, \tag{4}$$

where $\dot{m}_{nom}$ is the liquid mass flow rate and N_{ho} is the number of tray holes (N_{ho} = 68). Using C = 0.77 (from CFD simulation) h_{av} results 112 mm, being quite less than the spilling limit of 230 mm imposed by the gas chimneys.
Figure 13 shows the liquid volume fraction (on the left), the liquid velocity (on the center) and the gas velocity (on the right) at the mean cross sectional plane. Note that even thought the inlet distributor sprays liquid over chimneys, liquid only flows through the tray holes (sinks and sources). Sloshing is not strong, so the liquid level height is almost constant except where jets directly impact over the free surface of liquid.

Copyright © 2009 Asociación Argentina de Mecánica Computacional http://www.amcaonline.org.ar

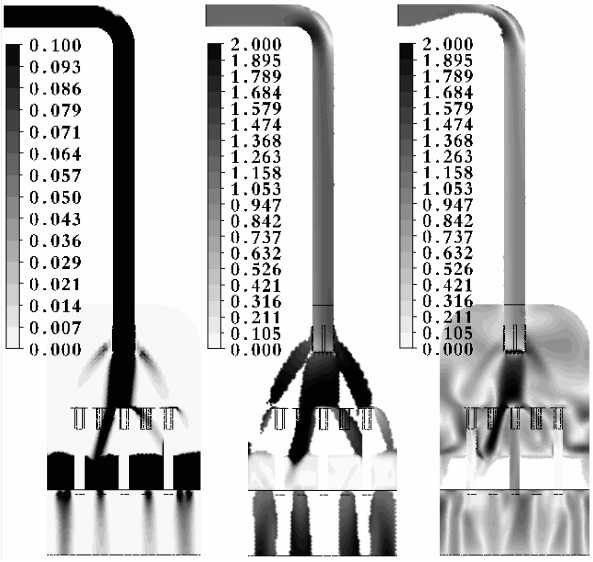

Figure 13: Results at the mean cross sectional plane. Left: liquid volume fraction. Center: liquid velocity. Right: gas velocity.

Figure 14 shows the time-average liquid mass flow rate through each one of the 68 tray holes (averaged along the last 1000 time steps, representing a time period of 5 sec.). Holes were grouped by dividing the tray in 4 quarters as showed in Figure 14 on the upper right side. Note that the mass flow rates range between 4.977×10^{-2} and 5.202×10^{-2} kg/sec., being the average equal to 5.0695×10^{-2} kg/sec. (represented by the horizontal dashed line). The standard deviation was only 5.1272×10^{-2} kg/sec., pointing out that the mass flow rate of either hole differs in less than 2% with respect to the average.

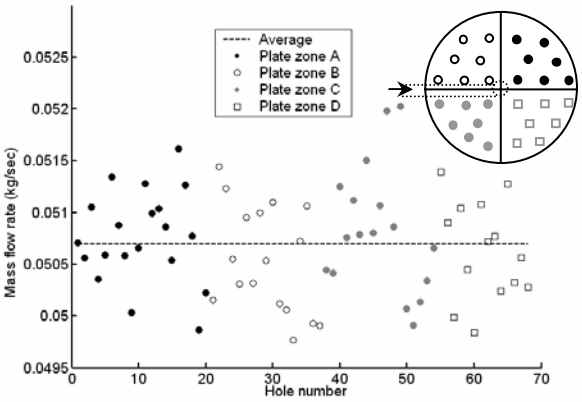

Figure 14: Mass flow rate through the tray holes.

Figure 15 shows the liquid volume fraction at two distances below the tray; the left picture correspond to a cross sectional plane at the middle between the tray and the ceramic-ball bed, while the right picture correspond to the top of the ceramic-ball bed. As noted, liquid does not wet the reactor edge and below the chimneys. As expected liquid trajectories are fairly verticals. That can be explained by two reasons; firstly the flow velocity through holes is not

Copyright © 2009 Asociación Argentina de Mecánica Computacional http://www.amcaonline.org.ar

enough to cause flashing or spraying. Secondly, the gas flow rate is negligible to alter the trajectory of the liquid jets. This allows a simple estimation of the behavior of the tray distributor under different operating conditions and under plugging situations where one or several holes are obstructed.

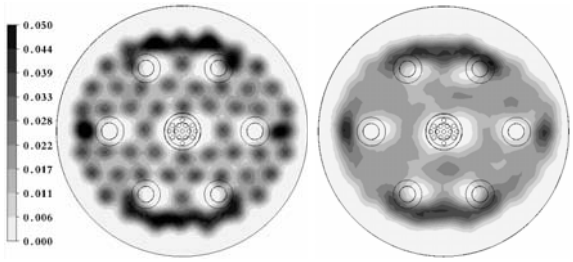

Figure 15. Liquid volume fraction. Left: at a cross sectional plane at 125 mm above the tray. Right: at the top of the ceramic-ball bed.

Figure 16 shows the area fraction (at the top of the ceramic ball bed) that is wetted by taking different wetted criteria. A criterion of 100% means that this surface receives a liquid flux $\varnothing_h = \dot{m}_T / A_T$ were $\dot{m}_T$ is the total mass flow rate and A_T is the cross transversal area of the bed. In Figure 16 curve shows that around the 50% of surface is wetted with $\varnothing_h$, while around 65% is wetted with at less 50% of $\varnothing_h$. In the same figure are also included the results corresponding to the TBR design operating conditions, for which the mass flow rate of both phases is increased approximately 25% with respect to the current operating conditions. Note that the evolution of the efficiently-wetted area is almost the same for both operating conditions indicating that the low reactor efficiency can not be explained by a wrong reactor operation.

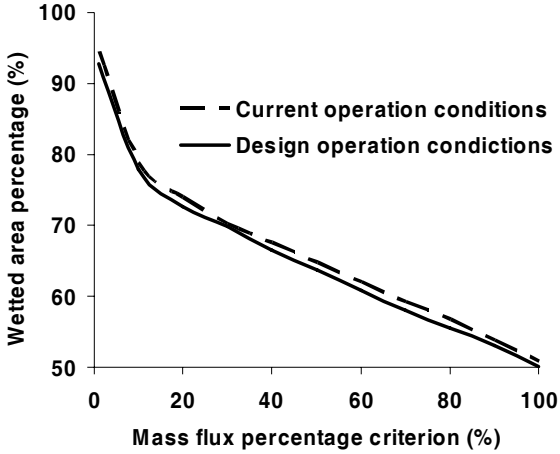

Figure 16: Wetted area percentage as a function of a cut criterion based on a percentage of average liquid mass flux.

Figure 17 shows the mass flow rate for both phases through each one of the 7 chimneys of the tray. As noted, gas flow down mainly through chimneys 3 and 4, while a significant amount of gas flow up through the central chimney. Gas recirculation is around 30 times more intense than the net mass flow rate of gas (4.0353×10^{-4} kg/sec.). Of course, this behavior is unexpected

Copyright © 2009 Asociación Argentina de Mecánica Computacional http://www.amcaonline.org.ar

because the tray was not designed to promote this effect, but due to the low gas flow intensity, the liquid flow impacting over the top of certain chimneys induces quite low pressure gradients that are enough to produce upward gas flows.

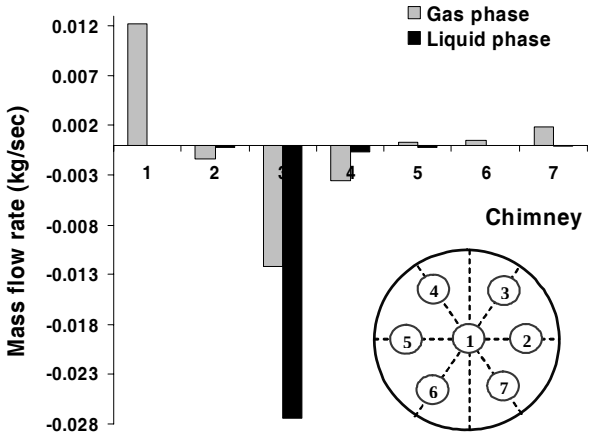

Figure 17: Mass flow rate of the liquid and gas phases through the chimneys.

3.4 Some possible scenarios that could explain the low efficiency of the TBR

From bibliography about trickle bed reactor distributors, it is clear that perforated-plate trays have lower efficiency than other technologies like chimney trays, bubble trays or vapor lift trays (VLT). The major disadvantage of perforated-plate trays is the high tendency to fouling and plugging due to the obstruction of some holes with coke, corrosion products or other debris carried into the reactor by the feed. Another important cause of low efficiency are small tray unevenness, that can originate that some holes flow more liquid than others (Alvarez et al., 2007; Maiti et al., 2007). From Eq. (4) it is possible to estimate the liquid-level height h_{av} as a function of the amount of obstructed holes. Figure 18 shows the evolution of h_{av} while holes obstructs along with the limit height until liquid begin to flow through the gas chimneys. As noted at less 20 holes have to be obstructed to arise to this situation.

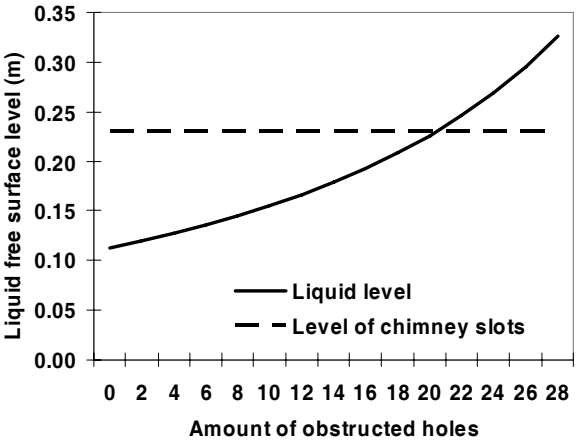

Figure 18: Liquid level height as a function of the amount of obstructed holes.

Copyright © 2009 Asociación Argentina de Mecánica Computacional http://www.amcaonline.org.ar

From simulations liquid drops nearly vertical below holes, so it is very likely that a significant fraction of the ceramic-ball bed would be poorly wetted if some holes near gas chimneys are plugged.

3.5 Effect of the ceramic-ball bed on wetting efficiency

The ceramic-ball bed improves the distribution of liquid before it enters to the catalyst bed. Besides, it enhances reactant mixture. For these reasons it is necessary to quantify its effect. Alvarez et al. (2007) suggested a simple expression to estimate the radial diffusion of the liquid inside a ball bed:

$$l_d = \sqrt{z.k_H \sqrt{d_p}}\ , \qquad (5)$$

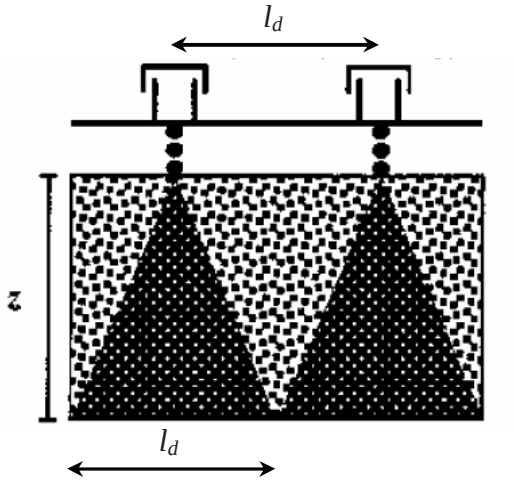

where l_d is the cone wet diameter, z is the bed height (150 mm), d_p is the ball diameter and k_H is a constant parameter. As noted from Eq. (5), the radial diffusion is proportional to contant k_H (k_H must be hold below 4 to guarantee homogeneous distribution). Assuming that liquid drops from the tray almost vertically and applying Eq. (5), it is easy to estimate the amount of drip points (holes) that wets each point of the catalyst bed. Figure 19 shows it for k_H equal to 2 and 4.

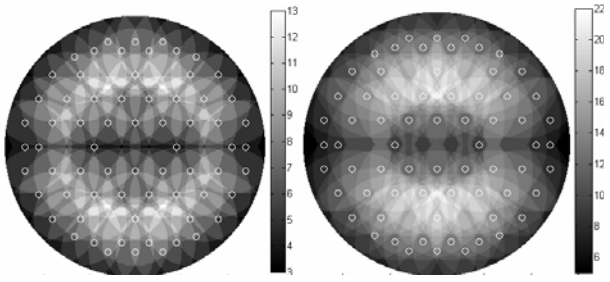

Figure 19: Number of drip points (holes) that wets each point of the catalyst bed. Left: k_H = 2. Right: k_H = 4.

3.6 Tray geometry modifications

CFD results pointed out that the non homogenous liquid distribution could explain the loss of reactor efficiency. Moreover, the influence of gas over the TBR fluid dynamic behavior is negligible. Then it is possible to propose two geometric modifications in order to improve liquid distribution; firstly to reduce the amount of gas chimneys to only one (the central

Copyright © 2009 Asociación Argentina de Mecánica Computacional http://www.amcaonline.org.ar

chimney), adding more drip point for liquid discharge. With one gas chimney the gas mean velocity will be less than 0.22 m/sec. and gas recirculation will disappear. Secondly, to replace the holes by short risers of around 50 mm height, in order to reduce plugging problems and the amount of plant shutdown for maintenance.

Figure 20 shows the amount of drip (holes) that wets each point of the catalyst bed by adding 6 drip at the location of the removed chimneys and 2 additional drips close to the central chimney. For this new tray the average amount of cones that wets each point of the catalyst bed increases from 7.3 to 8.7 and from 12.9 to 15.5 for $k_H = 2$ and $k_H = 4$ respectively.

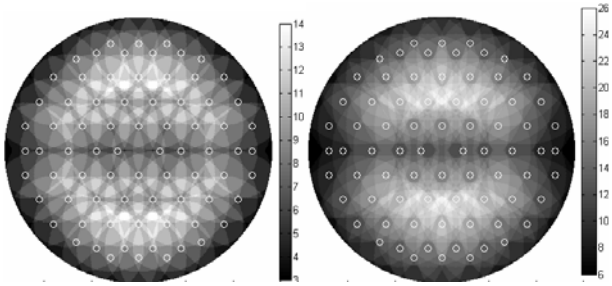

Figure 20: Number of drip points (holes) that wets each point of the catalyst bed when 8 drips are added. Left: $k_H = 2$. Right: $k_H = 4$.

Figure 21 shows the average and the standard deviation of the amount of drip points that impinge each point of the catalyst bed in function of the constant k_H for the current and the modified tray. Note that standard deviation increases slowly with k_H.

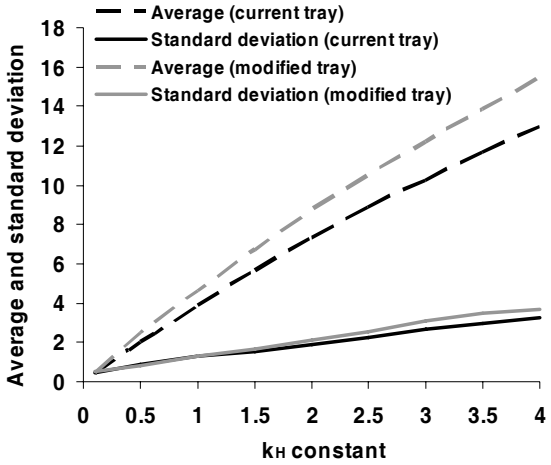

Figure 21: Average and standard deviation of the amount of drip points that wets each point of the catalyst bed as a function of the k_H.

4 CONCLUSIONS

A two-phase turbulent flow in the entry device of an industrial TBR was simulated by CFD. The wetting efficiency and liquid flow distribution was studied in deep, which lead to the following conclusions:

Copyright © 2009 Asociación Argentina de Mecánica Computacional http://www.amcaonline.org.ar

a- the use of sinks and sources seems to be a suitable option for modeling the tray-holes behavior. The shape constant coefficient for flow discharge modeling can be obtained by numeric and experimental tests

b- the liquid level height over the tray is quite constant, so all holes have a similar behavior. The liquid jet below the holes is roughly vertical and gas does not affect liquid trajectories

c- assuming that the liquid distribution inside the ceramic-ball bed can be estimated by Eq. (5), it is easy to estimate the effect of some operative or constructive modifications of the tray without the necessity of additional CFD simulations

d- two simple constructive modifications are proposed; to reduce the amount of gas chimneys to only one, adding some additional drips, and to change the current tray holes by short risers in order to reduce plugging problems.

5 KNOWLEDGEMENTS

Authors want to thanks to CONICET (grant 5271/05), ANPCyT (grant PICT 01141/2007), UNL (grant CAI+D 2009 Tipo II PI-65-333). Also they are gratefully to CTA, YPF S.A. to proportionate the industrial data and the plant experience required to carry out this research.

6 REFERENCES

Alvarez A., Ramírez S., Ancheyta J. and Rodríguez L., Key Role of Reactor Internals inHydroprocessing of Oil Fractions, *American Chemical Society*, 2007.

Atta A., Roy S. and Nigam K., Investigation of liquid maldistribution in trickle-bed reactors using porous media concept in CFD, *Chem. Eng. Science*, 62:7033-7044, 2007.

Bingham E. and Nelson D., Practical advances in petroleum processing, *chapter 13: Advanced reactor internals for hydroprocessing units*, Springer New Cork, 2006.

Dally, J. W., W. F. Riley, and K. G. McConnell, *Instrumentation for Engineering Measurements*, John Wiley and Sons, Inc. 2ed., 1993.

Gunjal P., Kashid M., Ranade V. and Chaudhari R., Hydrodynamics of trickle-bed reactors: experiments and CFD modeling, *Ind. Eng. Chem. Res.*, 44:6278-6294, 2005.

Harter I, Boyer C., Raynal L., Ferschneider G. and Gauthier T., Flow distribution studies applied to deep hydro-desulfurization, *Ind. Eng. Chem. Res.*40:5262-5267, 2001.

Jafari A., Zamankhan P., Mousavi S. and Pietarinen K, Modeling and CFD simulation of flow behavior and dispersivity through randomly packed bed reactors, *Chem. Eng. J.*, 144:476-482, 2008.

Kundu A., Saroha A. and Nigam K., Liquid distribution studies in trickle-bed reactors, *Chem. Eng. Science*, 56:5963-5967, 2001.

Maiti R. and Nigam K., Gas-liquid distributors for trickle bed reactors: a review, *American Chem. Society*, 6164-6182, 2007.

Lopes R. and Quinta-Ferreira R., Three-dimensional numerical simulation of pressure drop and liquid holdup for high-pressure trickle-bed reactor, *Chem. Eng. J.*, 145:112-120, 2008.

Perry, *Chemical Engineers' Handbook*, 6 ed., McGraw-Hill Co., 1984.

Ranade V., *Computational flow modeling for chemical reactor engineering*, Academic Press, 2002.

Storti M, Nigro N. and Paz R., PETSc-FEM a general purpose, parallel, multy-physics fem

Copyright © 2009 Asociación Argentina de Mecánica Computacional http://www.amcaonline.org.ar

program, International Center of Computational Method in Engineering (CIMEC), Argentina http://www.cimec.org.ar/petscfem, 2002.

Sonzogni, V., Yommi, A., Nigro, N., and Storti, M., A parallel finite element program on a Beowulf Cluster, *Advances in Engineering Software*, 33:427-443, 2002.

Zanotti A., Méndez C, Nigro N. and Storti M., A Preconditioning Mass Matrix to Avoid the Ill-Posed Two-Fluid Model, *ASME Journal of Applied Mechanics*, 74:4:732-740, 2007.

Copyright © 2009 Asociación Argentina de Mecánica Computacional http://www.amcaonline.org.ar